RSC Advances

ROYAL SOCIETY OF CHEMISTRY

www.rsc.org/advances

A variety of metal-organic and supramolecular networks constructed from a new flexible multifunctional building block bearing picolinate and terephthalate functionalities: hydrothermal self-assembly, structural features, magnetic and luminescent properties

Yong-Liang Shao,[a] Yan-Hui Cui,[a] Jin-Zhong Gu,*[a] Alexander M. Kirillov,[b] Jiang Wu [a] and Ya-Wen Wang*[a]

[a] *Key Laboratory of Nonferrous Metal Chemistry and Resources Utilization of Gansu Province, College of Chemistry and Chemical Engineering, Lanzhou University, Lanzhou 730000, P. R. China*

[b] *Centro de Química Estrutural, Complexo I, Instituto Superior Técnico, Universidade de Lisboa, Av. Rovisco Pais, 1049-001, Lisbon, Portugal*

* Corresponding author. Fax: +86 931 8915196. *E-mail address*: gujzh@lzu.edu.cn (J.-Z. Gu); ywwang@lzu.edu.cn (Y.-W. Wang).

Abstract

A novel flexible multifunctional building block (H_3L) bearing picolinate and terephthalate functionalities was designed and applied for the hydrothermal self-assembly generation of a series of coordination compounds $[Co(H_2L)_2(H_2O)_2]$ (**1**), $[M(HL)(H_2O)]_n$ {M = Cd (**2**) and Mn (**3**)}, $\{[Mn_{1.5}(L)(phen)(H_2O)_2]\cdot H_2O\}_n$ (**4**), $[Zn_3(L)_2(H_2O)_6]_n$ (**5**), and $\{[Zn_3(L)_2(py)(H_2O)_4]\cdot 4H_2O\}_n$ (**6**) {wherein H_3L = 2-(4-carboxypyridin-3-yl)terephthalic acid, phen = 1,10-phenanthroline, py = pyridine}. All the obtained products **1**–**6** were fully characterized by IR spectroscopy, elemental, thermogravimetric, powder and single-crystal X-ray diffraction analyses. By adjusting the molar ratio of NaOH and H_3L ligand, the latter becomes partially deprotonated to form the H_2L^- blocks in **1** and HL^{2-} moieties in **2** and **3**, or completely deprotonated to create the L^{3-} units in **4**–**6**. The structures of the obtained compounds range from a discrete 0D monomer **1** and 1D coordination polymers **4** and **5** to 2D coordination polymers **2** and **3**, and an intricate 3D metal-organic framework **6**; their detailed topological classification was also performed. The structures of **1**–**5** are further extended [0D→3D (**1**), 1D→3D (**4**, **5**), and 2D→3D (**2**, **3**)] into supramolecular networks by means of multiple hydrogen bonds. The results reveal that the nature of metal(II) ion, molar ratio between NaOH and H_3L ligand, and the presence (optional) of auxiliary ligand play a significant role in determining dimensionality, topology and other structural features of the obtained products. Magnetic susceptibility measurements indicate that compounds **3** and **4** have dominating antiferromagnetic couplings between metal centers. Furthermore,

luminescent properties of **2**, **5**, and **6** were also investigated.

Introduction

In recent years, the design of new metal-organic and supramolecular networks has become of high interest owing to vast variety of their structural architectures, topological characteristics, and different applications as functional materials.[1–10] However, it is still a great challenge to generate compounds with desirable structural features and properties, since a multitude of factors can influence the result, such as coordination geometries of metal nodes, connectivity of main organic ligands due to the presence of distinct functional groups, introduction of auxiliary ligands, variation in reaction temperatures, ratios of reagents, types of solvents, pH values, crystallization conditions, *etc*.[11–15] In this regard, diverse multicarboxylic or heterocyclic carboxylic acids are commonly applied as multifunctional building blocks in generating metal-organic networks, not only because of their ability to lead to different coordination modes and exhibit high thermal stability, but also due to their possibility to act as good H-bond donors and acceptors, thus allowing an additional supramolecular level stabilization of resulting compounds.[16–25] Apart from multifunctional carboxylate ligands, 1,10-phenanthroline (phen) and pyridine (py) are frequently applied as simple secondary N-donor building blocks to tune the coordination environment and stabilize structures, because of their efficient π···π stacking and H-bonding interactions.[16,17,26,27]

Being interested in the exploration of new multifunctional polycarboxylate building

blocks for the synthesis of metal-organic and supramolecular networks, we have designed a novel flexible multifunctional building block containing both chelating picolinate and linking terephthalate functionalities, namely 2-(4-carboxypyridin-3-yl)terephthalic acid (H_3L). Then, we have probed the hydrothermal self-assembly reactions of different metal(II) chlorides (M = Co, Cd, Mn, and Zn) with H_3L as a principal building block, along with optional 1,10-phenanthroline (phen) or pyridine (py) auxiliary ligands. The choice of these reactants was governed by the following considerations. (1) The coordination chemistry of H_3L is virtually unexplored, as confirmed by a search of Cambridge Crystallographic Database (CSD) that disclosed no structurally characterized compounds derived from this organic building block. (2) H_3L comprises three carboxylic groups that can become partially or completely deprotonated, depending on the molar ratio of NaOH and H_3L ligand. (3) In addition, H_3L contains a pyridyl and a phenyl ring with structural flexibility and conformation freedom; rotation of the C–C single bond between the aromatic rings can lead to various coordination geometries of metal ions. Thus, the potential coordination sites, one nitrogen atom from pyridyl ring and six oxygen atoms of three carboxylate groups, may supply anions with three different compensating charges and various acidity-dependent coordination modes. (4) The addition into the reaction system of an N-donor auxiliary ligand may improve the crystallization of metal-organic networks and reinforce their structures.

Thus, in the present study, we have generated by a hydrothermal self-assembly

protocol a series of new coordination compounds **1**–**6**, namely a discrete 0D complex $[Co(H_2L)_2(H_2O)_2]$ (**1**), 1D coordination polymers $\{[Mn_{1.5}(L)(phen)(H_2O)_2]\cdot H_2O\}_n$ (**4**) and $[Zn_3(L)_2(H_2O)_6]_n$ (**5**), 2D coordination polymers $[M(HL)(H_2O)]_n$ (M = Cd (**2**), and Mn (**3**)), and a 3D metal-organic framework $\{[Zn_3(L)_2(py)(H_2O)_4]\cdot 4H_2O\}_n$ (**6**). To our knowledge, these products represent the first coordination compounds obtained from H_3L. Their structural diversity suggests that the molar ratio of NaOH and H_3L ligand, type of metal node and presence of auxiliary ligand play an important role in the generation, structural and topological characteristics of **1**–**6**. The study thus reports the characterization of **1**–**6** by IR spectroscopy, elemental, thermogravimetric, powder and single-crystal X-ray diffraction, and topological analyses. In addition, magnetic (for **3** and **4**) and luminescent (for **2**, **5** and **6**) properties were investigated.

Scheme 1

Experimental

Materials and methods

All chemicals and solvents were of A.R. grade and obtained from commercial sources and used without further purification. 2-(4-Carboxypyridin-3-yl)terephthalic acid (H_3L) was synthesized by adopting a related procedure.[28,29] ^1H and ^{13}C NMR spectra were performed on a Bruker Advance III 400 spectrometer. Carbon, hydrogen and nitrogen content in **1**–**6** was determined using an Elementar Vario EL elemental analyzer. IR spectra were recorded using KBr pellets and a Bruker EQUINOX 55 spectrometer. Thermogravimetric analysis (TGA) was performed under N_2

atmosphere with a heating rate of 10 °C/min on a LINSEIS STA PT1600 thermal analyzer. Powder X-ray diffraction patterns (PXRD) were determined with a Rigaku-Dmax 2400 diffractometer using Cu-*K*α radiation (λ = 1.54060 Å), in which the X-ray tube was operated at 40 kV and 40 mV. Magnetic susceptibility data were collected in the 2–300 K temperature range with a Quantum Design SQUID Magnetometer MPMS XL-7 with a field of 0.1 T. A correction was made for the diamagnetic contribution prior to data analysis. Excitation and emission spectra were recorded for the solid samples on an Edinburgh FLS920 fluorescence spectrometer at room temperature.

2-(4-Carboxypyridin-3-yl)terephthalic acid (H_3L)

A mixture of ethyl 5-bromonicotinate (115.0 mg, 0.50 mmol), 2,5-bis(ethoxycarbonyl)phenylboronic acid (143.0 mg, 0.55 mmol), K_2CO_3 (210.0 mg, 1.5 mmol), $Pd(OAc)_2$ (56 mg, 0.025 mmol), and C_2H_5OH (50 mL) was stirred and refluxed for 10 h. After cooling to room temperature, the precipitate was filtered off, and the filtrate was concentrated under reduced pressure. The obtained residue was purified by silica gel column chromatography with dichloromethane/ethyl acetate (v/v 36 : 1) to give diethyl 2-(4-(ethoxycarbonyl)pyridin-3-yl)isophthalate as a white solid. A suspension of diester in 1 M NaOH was stirred at 80 °C for 2 h. The solution was cooled with ice and acidified with HCl to pH = 2.5. The white precipitate was collected to give H_3L in 41% yield based on ethyl 5-bromonicotinate. Calcd for $C_{14}H_9NO_6$: C 58.54, H 3.16, N 4.88%. Found: C 58.21, H 3.18, N 4.83%. IR (KBr, cm^{-1}): 1721 s, 1379 w, 1302 w, 1224 m, 1168 w, 1138 w, 1094 w, 1031 w, 918 w, 879

w, 804 w, 787 w, 764 w, 754 w, 730 w, 654 w. ^{1}H NMR (400 MHz, DMSO-d_6): δ 13.38 (s, 3H), δ 8.68 (s, 1H), δ 8.11 (t, 2H), δ 8.03-7.99 (m, 2H), δ 7.96-7.91 (m, 1H). ^{13}C NMR (100 MHz, DMSO-d_6): δ 167.9 (*C*OOH), 166.3 (*C*OOH), 166.0 (*C*OOH), 148.6, 147.1, 139.2, 137.6, 137.0, 135.3, 133.4, 131.4, 130.4, 129.3, 124.2 (aromatic *C*).

Synthesis of $[Co(H_2L)_2(H_2O)_2]$ (1)

A mixture of $CoCl_2{\cdot}6H_2O$ (71.0 mg, 0.3 mmol), H_3L (73.0 mg, 0.3 mmol), NaOH (12 mg, 0.3 mmol) and H_2O (10 mL) was stirred at room temperature for 15 min, then sealed in a 25 mL Teflon-lined stainless steel vessel, and heated at 160 °C for 3 days, followed by cooling to room temperature at a rate of 10 °C/h. Pink needle-shaped crystals were isolated manually, washed with distilled water and dried to give **1**. Yield: 35% (based on H_3L). Calcd for $C_{28}H_{20}CoN_2O_{14}$: C 50.39, H 3.02, N 4.20%. Found: C 50.78, H 2.83, N 4.41%. IR (KBr, cm^{-1}): 3420 w, 3046 m, 3067 w, 1716 s, 1699 s, 1613 m, 1598 s, 1563 m, 1398 m, 1314 w, 1267 w, 1256 w, 1176 w, 1134 m, 1035 w, 926 m, 866 m, 812 w, 801 w, 768 w, 755 m, 702 m, 646 w, 608 w, 542 w, 468 w.

Synthesis of $[M(HL)(H_2O)]_n$ (M = Cd (2) and Mn (3))

A mixture of $MCl_2{\cdot}xH_2O$ (x = 1 for **2** and x = 4 for **3**, 0.3 mmol), H_3L (73.0 mg, 0.3 mmol), NaOH (24 mg, 0.6 mmol) and H_2O (10 mL) was stirred at room temperature for 15 min, and then sealed in a 25 mL Teflon-lined stainless steel vessel, and heated at 160 °C for 3 days, followed by cooling to room temperature at a rate of 10 °C/h. Crystals of **2** and **3** were isolated manually and washed with distilled water. Yield: 70% for **2**, 60% for **3** (based on H_3L). Calcd for $C_{14}H_9CdNO_7$: C 40.46, H 2.18, N

3.37%. Found: C 40.11, H 2.43, N 3.67%. IR (KBr, cm^{-1}): 3407 w, 1712 m, 1618 s, 1585 s, 1557 m, 1527 w, 1482 m, 1378 s, 1296 w, 1273 w, 1242 w, 1149 s, 1033 w, 978 w, 906 w, 890 m, 868 w, 834 w, 809 w, 770 m, 704 w, 651 w, 562 m, 479 m. Calcd for $C_{14}H_9MnNO_7$ (**3**): C 46.95, H 2.53, N 3.91%. Found: C 47.36, H 2.47, N 3.85%. IR (KBr, cm^{-1}): 3406 w, 1713 s, 1621 s, 1586 s, 1557 s, 1482 w, 1390 s, 1299 w, 1242 s, 1147 w, 1121 m, 1044 w, 1032 m, 978 w, 948 w, 860 m, 814 m, 757 m, 748 w, 703 m, 662 w, 648 w, 567 m, 491 w, 476 w.

Synthesis of $\{[Mn_{1.5}(L)(phen)(H_2O)_2]\cdot H_2O\}_n$ (4)

A mixture of $MnCl_2\cdot 6H_2O$ (59.4 mg, 0.3 mmol), H_3L (72.0 mg, 0.3 mmol), phen (60.0 mg, 0.3 mmol), NaOH (36 mg, 0.9 mmol) and H_2O (10 mL) was stirred at room temperature for 15 min, then sealed in a 25 mL Teflon-lined stainless steel vessel, and heated at 160 °C for 3 days, followed by cooling to room temperature at a rate of 10 °C/h. Yellow block-shaped crystals were isolated manually, washed with distilled water and dried to give **4**. Yield: 50% (based on H_3L). Calcd for $C_{26}H_{20}Mn_{1.5}N_3O_9$: C 51.97, H 3.36, N 6.99%. Found: C 51.48, H 3.29, N 7.37%. IR (KBr, cm^{-1}): 3465 w, 1619 s, 1577 s, 1516 m, 1478 w, 1427 m, 1370 s, 1266 m, 1170 w, 1146 w, 1128 w, 1098 w, 1048 w, 1034 m, 985 w, 948 w, 928 w, 895 w, 847 s, 816 m, 777 s, 726 m, 708 m, 664 w, 637 w, 576 w, 554 w, 490 w, 464 w.

Synthesis of $[Zn_3(L)_2(H_2O)_6]_n$ (5)

A mixture of $ZnCl_2$ (41.0 mg, 0.3 mmol), H_3L (72.0 mg, 0.3 mmol), NaOH (36 mg, 0.9 mmol) and H_2O (10 mL) was stirred at room temperature for 15 min, then sealed in a 25 mL Teflon-lined stainless steel vessel, and heated at 160 °C for 3 days,

followed by cooling to room temperature at a rate of 10 °C/h. Colorless block-shaped crystals were isolated manually, washed with distilled water and dried to give **5**. Yield: 50% (based on H_3L). Calcd for $C_{28}H_{24}Zn_3N_2O_{18}$: C 38.53, H 2.77, N 3.21%. Found: C 38.84, H 2.49, N 3.38%. IR (KBr, cm^{-1}): 3416 m, 1617 s, 1566 s, 1484 m, 1412 s, 1378 s, 1300 m, 1268 w, 1250 w, 1142 w, 1051 w, 1040 w, 986 w, 937 w, 878 w, 838 m, 773 s, 701 w, 652 w, 578 w, 507 w.

Synthesis of $\{[Zn_3(L)_2(py)(H_2O)_4]\cdot 4H_2O\}_n$ (6)

The preparation of **6** was similar to that of **5** except using py (0.5 mL, 6.3 mmol) instead of NaOH. After being cooled to room temperature, colorless block-shaped crystals of **6** were isolated manually, and washed with distilled water. Yield: 50% (based on H_3L). Calcd for $C_{33}H_{33}Zn_3N_3O_{20}$: C 40.12, H 3.37, N 4.25%. Found: C 39.85, H 3.61, N 4.57%. IR (KBr, cm^{-1}): 3366 m, 1635 s, 1575 s, 1551 m, 1489 m, 1453 m, 1421 m, 1359 s, 1271 m, 1135 w, 1076 w, 1055 w, 1037 w, 927 w, 879 m, 845 m, 814 w, 786 w, 772 m, 701 m, 654 w, 582 w, 484 w.

X-ray crystal data collection and structure determination

The single-crystal X-ray data collection for **1**–**6** was performed on a Bruker Smart CCD diffractometer, using graphite-monochromated Mo K_α radiation (λ = 0.71073 Å). Semiempirical absorption corrections were applied using the SADABS program. The structures were solved by direct methods and refined by full-matrix least-squares on F^2 using the SHELXS-97 and SHELXL-97 programs.[30] All the non-hydrogen atoms were refined anisotropically by full-matrix least-squares methods on F^2. All the

hydrogen atoms (except those bound to water molecules) were placed in calculated positions with fixed isotropic thermal parameters and included in structure factor calculations at the final stage of full-matrix least-squares refinement. The hydrogen atoms of water molecules were located by difference maps and constrained to ride on their parent O atoms. The crystal data for **1**–**6** are summarized in Table 1 and selected bond lengths are listed in Table S1†. Hydrogen bonds in the compounds **1**–**6** are given in Table S2†.

Results and discussion

Crystal structures

Crystal structure of 1

The discrete 0D monomer **1** crystallizes in the monoclinic space group *P*21/*c*. Its asymmetric unit contains one Co(II) atom (half occupancy, located at an inversion center), one H_2L^- ligand, and one coordinated water molecule. As shown in Fig. 1a, the six-coordinate Co1 center is bound by two carboxylate O atoms and two N atoms in equatorial sites from two symmetry equivalent H_2L^- ligands (these are mutually *trans*) and two axial O atoms from two equivalent H_2O moieties, thus forming an ideal octahedral $\{CoN_2O_4\}$ geometry. The Co–N bonds are 2.071(2) Å, while the Co–O distances vary from 2.033(3) to 2.189(2) Å; all these distances are comparable to those found in the reported Co(II) compounds.[16,17] In **1**, the H_2L^- acts as a terminal ligand (Scheme 1, mode I), in which the deprotonated carboxylate group is in the $\eta^1{:}\eta^0$ monodentate mode. The dihedral angle between the pyridyl and phenyl rings in

the H_2L^- block is 59.95°. The discrete monomeric units of **1** are interlinked by the strong O–H···O hydrogen bonds to form a 3D supramolecular framework (Fig. 1b, Table S2, ESI†). For the sake of topological analysis, a concept of the simplified underlying net was followed.[27] Hence, the molecular $[Co(H_2L)_2(H_2O)_2]$ units were reduced to the respective centroids and considered as the 8-connected nodes. The obtained underlying framework (Fig. 1c) is a uninodal 8-connected 3D net with a rare 8T9 topology, which is defined by the point symbol of $(3^6.4^{10}.5^{11}.6)$.

Scheme 2

Fig. 1

Crystal structures of 2 and 3

Single-crystal X-ray analyses reveal that compounds **2** and **3** are isostructural; the structure of **2** is described in detail as a representative example (Fig. 2). The asymmetric unit of **2** contains two crystallographically unique Cd(II) atoms (Cd1 and Cd2 with half occupancy, they are located on a 2-fold rotation axis), one HL^{2-} ligand, and one H_2O moiety. As depicted in Fig. 2a, the Cd1 center is coordinated by four O and two N atoms from the four different HL^{2-} blocks and possesses a distorted octahedral $\{CdN_2O_4\}$ coordination environment with the equatorial plane defined by the pairs of O1 and O1iii (mutually *cis*), and N1i and N1ii atoms (mutually *cis*); the axial positions are taken by the O5i and O5ii atoms. The six-coordinate Cd2 center reveals a distorted octahedral $\{CdO_6\}$ geometry, filled by the pairs of carboxylate O2/O2iv (mutually *trans*) and O5ii/O5v (mutually *cis*) atoms, and a pair of water ligands O7/O7iv (mutually *cis*). The Cd–O [2.218(2)–2.423(2) Å] and Cd–N [2.324(2)

Å] bond lengths are in good agreement with those observed in some other related Cd(II) compounds.[16,17] In **2**, the HL^{2-} spacer exhibits a μ_4-coordination mode (Scheme 1, mode II), in which the two deprotonated carboxylate groups show the μ_2-η^1:η^1 and μ_2-η^2:η^0 bidentate modes. The dihedral angle between the pyridyl and phenyl rings in HL^{2-} is 55.37°. The HL^{2-} moieties alternately link the adjacent Cd(II) centers to form a 1D chain motif with the Cd···Cd separation of 4.003(2) Å (Fig. 2b). These 1D motifs are arranged into a 2D sheet structure by further coordination interactions of the HL^{2-} ligands to Cd(II) ions (Fig. 2b). For topological analysis,[31] the 2D metal-organic network in **2** was simplified (terminal H_2O ligands omitted, μ_4-HL^{2-} moieties reduced to centroids) to give an underlying binodal 4,4-connected layer (Fig. 2d). It is built from the 4-connected topologically equivalent Cd1/Cd2 and μ_4-HL^{2-} nodes and features an undocumented topology[31–33] defined by the point symbol of $(4^3.6^2.8)$. The novelty of this topology was confirmed by a search of different databases.[31–33] Furthermore, the neighboring metal-organic sheets in **2** are assembled, through the O–H···O hydrogen bonds, into a complex 3D supramolecular framework (Fig. 2c).

Fig. 2

Crystal structure of 4

This compound crystallizes in the triclinic space group *P*–1 and features a linear 1D metal-organic chain structure (Fig. 3). The asymmetric unit bears two crystallographically independent Mn(II) atoms (Mn1 with full occupancy; Mn2 with half-occupancy, located at an inversion center), one L^{3-} and one phen ligand, two H_2O

ligands and two water molecules of crystallization. As depicted in Fig. 3a, the six-coordinate Mn1 atom adopts a distorted octahedral {MnN_3O_3} geometry in which the equatorial plane is provided by the N2 and N3 atoms from phen ligand and the N1 and one O3i atoms (mutually *cis*) of two different L^{3-} blocks, while the O1 atom from the L^{3-} moiety and the O7 water ligand occupy the axial positions. The six-coordinate Mn2 atom possesses a slightly distorted octahedral {MnO_6} coordination environment, filled by the pairs of carboxylate O4/O4iv and O5ii/O5iii atoms, and a pair of O8/O8iv water ligands; within each pair, the symmetry equivalent atoms are in mutually *trans* positions. The Mn–O [2.103(3)–2.210(3) Å] and Mn–N [2.243(3)–2.336(3) Å] bond lengths are in good agreement with those observed in some other Mn(II) compounds.[16,17] In **4**, the L^{3-} ligands show a μ_4-coordination mode (Scheme 1, mode III), in which the carboxylate groups are either η^1:η^0 monodentate or η^1:η^1 bidentate. The dihedral angle between the pyridyl and phenyl rings in the L^{3-} ligand is 52.09°. The three neighboring Mn(II) ions are bridged by means of two carboxylate groups from the two different L^{3-} moieties, giving rise to a centro-symmetric trinuclear Mn(II) subunit (Fig. 3b). In this trimanganese(II) unit, the Mn···Mn distance of 4.954(3) Å is significantly longer than those reported for other carboxylate-bridged trinuclear Mn(II) complexes.[17,30] The adjacent Mn_3 subunits are further linked by L^{3-} blocks into a 1D chain (Fig. 3b), having the shortest distance of 10.388(3) Å between the neighboring Mn_3 units. For the sake of topological analysis, an underlying 1D metal-organic network of **4** was obtained upon reducing the μ_4-L ligands to their centroids and eliminating terminal H_2O and phen moieties, thus giving

rise to a binodal 4,4-connected chain (Fig. 3d). Interestingly, this chain possesses an unreported topology[29–31] defined by the point symbol of $(3^2.4.5^2.6)_2(3^2.4^2.5^2)$, wherein the $(3^2.4.5^2.6)$ and $(3^2.4^2.5^2)$ indices correspond to the μ_4-L and Mn2 nodes, respectively. Besides, the 1D coordination chains are held into a 2D network by H-bonding interactions and also involving crystallization H_2O molecules (Table S2†). It is further extended into a 3D supramolecular framework by π–π stacking interactions (Fig. 3c).

Fig. 3

Crystal structure of 5

The compound **5** crystallizes in the monoclinic space group *C*2/*c* and also features a linear 1D metal-organic chain structure (Fig. 4). In the asymmetric unit, there are two crystallographically independent Zn(II) atoms (Zn1 with full occupancy; Zn2 with half occupancy, located on a 2-fold rotation axis), one L^{3-} and three coordinated water molecules. As depicted in Fig. 4a, the four-coordinate Zn1 atom adopts a distorted $\{ZnO_4\}$ tetrahedral geometry, filled by two O atoms from two different L^{3-} ligands and two O atoms from two coordinated H_2O molecules. The six-coordinate Zn2 atom adopts a distorted $\{ZnN_2O_4\}$ octahedral geometry in which the equatorial sites are taken by a pair of O6/O6ii atoms (mutually *cis*) from two different L^{3-} ligands and a pair of O9/O9ii atoms (mutually *cis*) from two coordinated water molecules, while the N1 and N1ii atoms of two individual L^{3-} blocks occupy the axial positions. The Zn–O and Zn–N bond lengths are in the range of 1.935(2)–2.118(3) and 2.127(3) Å, respectively. In **5**, the L^{3-} ligands show a μ_3-coordination mode (Scheme 1, mode IV),

in which all carboxylate groups are η^1:η^0 monodentate. The dihedral angle between the pyridyl and phenyl rings in the L^{3-} ligand is 66.62°. The carboxylate groups of the L^{3-} blocks alternately bridge neighboring Zn(II) atoms to form a ladder-like coordination chain (Fig. 4b). It was analyzed from a topological viewpoint following the concept of the simplified underlying net.[31,35] After eliminating terminal H_2O ligands and contracting the μ_3-L spacers to their centroids, a uninodal underlying chain was generated (Fig. 4d). It is composed of the 3-connected μ_3-L nodes and 2-connected Zn1/Zn2 linkers, disclosing the SP 1-periodic net (4,4)(0,2) topology with the point symbol of $(4^2.6)$.[31] The adjacent 1D coordination chains are further extended (1D→3D) by multiple hydrogen bonds (Fig. 4c, Table S2†) into a supramolecular framework.

Fig. 4

Crystal structure of 6

The asymmetric unit of **6** consists of two symmetry non-equivalent Zn(II) atoms (Zn1 with full occupancy; Zn2 with half occupancy, located on a 2-fold rotation axis), one μ_4-L^{3-} ligand, a half of py moiety, two H_2O ligands and two water molecules of crystallization. As depicted in Fig. 5a, both Zn1 and Zn2 atoms are five-coordinate and possess a $\{ZnNO_4\}$ trigonal-bipyramid environment. The Zn1 atom is coordinated by three O and one N atom from the three different L^{3-} blocks, and one O atom from one coordinated H_2O molecule. The Zn2 atom is bound by two O atoms from two different L^{3-} ligands, one N atom from one py moiety, and two O atoms from two coordinated water molecules. The Zn–O and Zn–N bond lengths are in the

range of 1.957(3)–2.147(4) and 2.053(6)–2.065(4) Å, respectively. All the Zn–O and Zn–N distances in **5** and **6** are comparable to those in other reported Zn(II) compounds.[16–18] In **6**, the L^{3-} ligands show a μ_4-coordination mode (Scheme 1, mode V), in which two carboxylate groups are η^1:η^0 monodentate and the third group is μ_2-η^1:η^1 bidentate. The dihedral angle between the pyridyl and phenyl rings in the L^{3-} ligand is 51.68°. The carboxylate groups of the L^{3-} ligands multiply bridge the adjacent Zn(II) ions to form a complex 3D open metal-organic framework (Fig. 5b). It features channels [13.75 × 4.923 Å measured by atom-to-atom distances], which are filled with water molecules of crystallization. If seen down the *c* axis (Fig. 5c), the framework of **6** also displays channels with a size of *ca*. 9.574 × 5.192 Å measured by atom-to-atom distances. Upon removal of water molecules of crystallization, we computed by PLATON an effective free volume that is 10.2% of the crystal volume.[36] However, after eliminating both coordinated and guest water molecules, the effective free volume attains 12.5% of the crystal volume of **6**. In contrast to **5**, the 3D metal-organic structure of **6** is more complex due to the presence of μ_4-L blocks. To perform the topological classification, the metal-organic framework of **6** was simplified by omitting terminal H_2O and pyridine ligands and by reducing the μ_4-L blocks to their centroids. The obtained underlying 3D net is composed of the 2-connected Zn2 linkers, 3-connected Zn1 nodes, and 4-connected μ_4-L nodes (Fig. 5d). Its topological analysis[31] revealed a binodal 3,4-connected framework with the fsc-3,4-Pbcn-2 topology and the point symbol of $(6^3)(6^5.8)$, wherein the (6^3) and $(6^5.8)$ notations are those of Zn1 and μ_4-L nodes, respectively. The present topological type

is rather rare, as confirmed by a search of different databases.[31–33]

Coordination modes of 2-(4-carboxypyridin-3-yl)terephthalate blocks and structural comparison

As depicted in Scheme 2, the ligands derived from H_3L exhibit versatile coordination modes in compounds **1**–**6**. The H_3L block exists in partially and fully deprotonated forms, namely H_2L^-, HL^{2-} and L^{3-}, depending on the molar ratio of NaOH and H_3L ligand. For example, when the molar ratios of NaOH and H_3L are 1:1 and 2:1, the H_3L ligands become partially deprotonated to give H_2L^- and HL^{2-} forms in **1**–**3**. When the molar ratio of NaOH and H_3L is adjusted to 3:1, the ligand is completely deprotonated to afford the L^{3-} form in **4** and **5**. Five different coordination modes of ligands derived from H_3L were observed in compounds **1**–**6**, in which the carboxylate groups adopt three typical modes, that is, η^1:η^0 monodentate and μ_2-η^2:η^0 and μ_2-η^1:η^1 bidentate modes. The pyridyl N atom of the principal ligand always acts as a donor to metal ions in **1**–**6**, reinforcing the binding of the adjacent carboxylate group. To facilitate the generation of a certain coordination environment around metal ions in the assembly process, the C–C single bond between the pyridyl and phenyl rings of the H_2L^-, HL^{2-} or L^{3-} ligand can relatively freely rotate, with the corresponding dihedral angles being in the range of 51.68–66.62º. The obtained results indicate that the ligands derived from H_3L can adopt various coordination modes to meet the central metal ions in the compounds, and behave as either terminal (in **1**) or different μ_3- (in **5**) and μ_4-building blocks (in **2**, **3**, **4**, and **6**).

Apart from different dimensionality of metal-organic networks that ranges from 0D (in **1**) and 1D (in **4** and **5**) to 2D (in **2** and **3**) and 3D (in **6**), all the obtained products also reveal distinct topologies, including their rare or even unprecedented types. In fact, the topological analysis of the coordination networks disclosed: (i) a uninodal 3-connected 1D chain with the SP 1-periodic net (4,4)(0,2) topology in **5**, (ii) a binodal 3,4-connected 3D framework with a rare fsc-3,4-Pbcn-2 topology in **6**, and (iii) a binodal 4,4-connected 1D chain in **4** or 2D layer in **2** and **3** with the unique topologies. A rare 8T9 topology was also identified in a 3D supramolecular network in **1**.

It should also be mentioned that while attempting the hydrothermal self-assembly syntheses of compounds **1**–**6**, the reactions of different metal(II) chlorides with H_3L as a single building block and also in the presence of an ancillary ligand (phen or py) were tested. Only in the case of **4** and **6**, the incorporation of phen and py moieties occurred. In other cases, we were not able to obtain crystalline samples of sufficient quality to be characterized by single crystal X-ray diffraction, or the reaction attempts were not successful. We predict that further optimization of reaction conditions might allow the introduction of various N-donor ancillary blocks (e.g., by substituting H_2O ligands in **1**–**3** and **5**), thus resulting in the generation of mixed-ligand coordination compounds. The exploration of H_3L as a versatile building block for the synthesis of mixed-ligand derivatives will be pursued.

Thermogravimetric analysis and PXRD results

The thermal stability of compounds **1**–**6** was studied under nitrogen atmosphere by thermogravimetric analysis (TGA) and the obtained plots are given in Fig. S1†. The compound **1** releases its two water ligands (exptl, 5.7%; calcd, 5.4%) in the

88–169 °C range, followed by the decomposition at 238 °C. The TGA curves of **2** and **3** indicate that there is one distinct thermal effect in the 131–194 and 138–194 °C range, respectively, which corresponds to the removal of one coordinated H_2O molecule (exptl, 4.7% (**2**), 5.4% (**3**); calcd, 4.3% (**2**), 5.0% (**3**)). Further heating up to 369 and 377 °C, respectively, leads to the decomposition of dehydrated samples. For **4**, the weight loss associated with the removal of two H_2O ligands and one water molecule of crystallization is observed in the 141–268 °C interval (exptl, 8.7%; calcd, 9.0%), and the decomposition of the remaining solid begins at 308 °C. For **5**, there is one distinct thermal effect in the 164–228 °C range that corresponds to the removal of six coordinated H_2O molecules (exptl, 12.2%; calcd, 12.4%). Further heating up to 336 °C leads to the decomposition of a dehydrated sample. Compound **6** loses its four lattice and four coordinated water molecules (exptl, 14.9%; calcd, 14.6%) in the 164–228 °C range, followed by decomposition at 388 °C.

Powder X-ray diffraction (PXRD) experiments for compounds **1**–**6** have been carried out at room temperature to identify whether the crystal structures can represent the bulk samples. As shown in Fig. S2†, the peak positions of the PXRD patterns closely match the simulated ones, thus indicating that the as-synthesized bulk materials are pure products.

Luminescent properties

The emission spectra of H_3L and its cadmium(II) and zinc(II) compounds **2**, **5** and **6** were recorded at room temperature in the solid state (Fig. 6). The uncoordinated H_3L exhibits a weak photoluminescence with an emission maximum at 454 nm if excited

at 365 nm. However, the metal-organic networks **2**, **5** and **6** reveal the substantially more intense emission bands with the maxima at 439 nm (λ_{ex} = 352 nm), 404 nm (λ_{ex} = 345 nm), and 430 nm (λ_{ex} = 341 nm), respectively. These bands are presumably associated with the intraligand ($\pi^* \rightarrow n$ or $\pi^* \rightarrow \pi$) emission.[37] The observed enhancement of luminescence in **2**, **5**, and **6** can depend on the type of ligands present in these compounds and their binding modes.[38] A stronger emission intensity in **6** over **2** and **5** can potentially be explained by structural differences in these compounds, namely because of higher dimensionality of **6** and the presence of auxiliary pyridine ligand.

Fig. 6

Magnetic properties

Variable-temperature magnetic susceptibility studies were carried out on powder samples of manganese(II) derivatives **3** and **4** in the 2–300 K temperature range. For **3**, as shown in Fig. 7, the $\chi_M T$ value at 300 K is 4.41 $cm^3 \cdot mol^{-1} \cdot K$, which is close to the value of 4.38 $cm^3 \cdot mol^{-1} \cdot K$ expected for one magnetically isolated high-spin Mn(II) center (S_{Mn} = 5/2, g = 2.0). The $\chi_M T$ values steadily decrease on lowering the temperature and reach the minimum of 0.176 $cm^3 \cdot mol^{-1} \cdot K$ at 2.00 K. Between 50 and 300 K, the magnetic susceptibility can be fitted to the Curie–Weiss law with C_M = 5.04 $cm^3 \cdot mol^{-1} \cdot K$ and θ = –42.9 K. These results indicate an antiferromagnetic interaction between the adjacent Mn(II) ions. According to the crystal structure of **3**, compound **3** can be considered as 1D chain from the viewpoint of magnetism. We tried to fit the magnetic data of **3** using the following expression[39] for a 1D Mn(II)

chain:

$\chi_{chain} = (Ng^2\beta^2/kT)[A + Bx^2][1 + Cx + Dx^3]^{-1}$

with $A = 2.9167$, $B = 208.04$, $C = 15.543$, $D = 2707.2$, and $x = |J|/kT$

Using this rough model, the susceptibilities for **3** were simulated, leading to J = –2.75 cm^{-1}, g = 2.06, and the agreement factor $R = 5.83 \times 10^{-6}$ ($R = \Sigma(\chi_{obs}T-\chi_{calc}T)^2/\Sigma(\chi_{obs}T)^2$). The J parameter confirms that an antiferromagnetic exchange coupling exists between the adjacent Mn(II) centers, which is agreement with a negative θ value.

Fig. 7

For **4**, the $\chi_M T$ value at 300 K is 6.60 $cm^3 \cdot mol^{-1} \cdot K$, which is close to the value of 6.57 $cm^3 \cdot mol^{-1} \cdot K$ expected for one and a half of magnetically isolated high-spin Mn(II) centers ($S_{Mn} = 5/2$, $g = 2.0$). Upon cooling, the $\chi_M T$ value drops down very slowly from 6.60 $cm^3 \cdot mol^{-1} \cdot K$ at 300 K to 6.42 $cm^3 \cdot mol^{-1} \cdot K$ at 104 K and then decreases steeply to 2.22 $cm^3 \cdot mol^{-1} \cdot K$ at 2 K (Fig. 8). The χ_M^{-1} *vs.* T plot for **4** in the 2–300 K interval obeys the Curie-Weiss law with a Weiss constant θ of –4.45 K and a Curie constant C of 6.71 $cm^3 \cdot mol^{-1} \cdot K$. The negative value of θ and the decrease of the $\chi_M T$ should be attributed to the overall antiferromagnetic coupling between the Mn(II) centers within the Mn_3 unit. According to the structure of compound **4**, there is one set of magnetic exchange pathway within the trinuclear cluster via carboxylate bridge (Fig. 3d). We tried to fit the magnetic data of **4** using the following expression[40] for the linear trinuclear Mn(II) motif:

$$\hat{H} = -2\sum_{i=1}^{n}\sum_{j>i}^{n} J_{ij}\vec{S}_i\vec{S}_j$$

$$\hat{H} = -2J_{12}\vec{S}_1\vec{S}_2 - 2J_{23}\vec{S}_2\vec{S}_3 - 2J_{13}\vec{S}_1\vec{S}_3$$

$$\chi_t = \frac{N\beta^2 g^2}{3kT} \times \frac{\sum_S S_T(S_T+1)(2S_T+1)e^{-E(S_T)/kT}}{\sum_S (2S_T+1)e^{-E(S_T)/kT}}$$

$$\chi_m = \frac{\chi_t}{1-(2zJ'/Ng^2\beta^2)\chi_t}$$

where $J_{12} = J_{23} = J_1$, $J_{13} = J_2$ (J_{12} and J_{23} are the exchange interactions between the "central" Mn(II) and two "outer" Mn(II) atoms; J_2 is the exchange interaction between the "outer" Mn(II) ions within a Mn_3 unit), zJ' refers to the intercluster coupling constant in the 1D chain. This model gives satisfactory results with the superexchange parameters: $J_1/k_B = -1.35$ K, $J_2/k_B = -0.45$ K, $zJ'/k_B = -0.18$ K, and $g = 2.01$. The agreement factor defined by $R = \Sigma(\chi_m T_{exp} - \chi_m T_{calc})^2/\Sigma(\chi_m T_{exp})^2$ is 9.86×10^{-4}. These values confirm the presence of antiferromagnetic interaction between the Mn(II) ions within a trinuclear subunit. The inercluster magnetic interaction (zJ') is rather small, indicating that the exchange interactions between two magnetic clusters are very weak, which is probably due to a long separation [10.388 (3) Å] of the adjacent magnetic subunits.

Fig. 8

Conclusions

In this work, by selecting different metal(II) nodes (M(II) = Co, Cd, Mn, Zn) and adjusting the molar ratio of NaOH and H_3L ligand and/or the type of the aromatic N-donor auxiliary ligand (optional), a new series of transition metal coordination compounds driven by the 2-(4-carboxypyridin-3-yl)terephthalic acid blocks were synthesized by the hydrothermal self-assembly method. The structures of the obtained

products vary from the 0D monomer (**1**) and 1D coordination chains (**4** and **5**) to 2D metal-organic layers (**2** and **3**) and 3D framework (**6**) with distinct architectures and topologies, including their unprecedented types. The structural diversity of **1**–**6** demonstrates that the molar ratio of NaOH and H_3L ligand and the nature of the metal ion and auxiliary ligand play a crucial role in the assembly of these distinct products which, to our knowledge,[33] represent the first coordination compounds derived from H_3L. Thus, the study also opens up the application of 2-(4-carboxypyridin-3-yl)terephthalic acid as a virtually unexplored but rather versatile multifunctional building block for the generation of diverse coordination compounds.

Electronic supplementary information (ESI) available: selected bonding (Table S1) and H-bonding (Table S2) distances, TGA plots (Fig. S1) and PXRD patterns (Fig. S2), and crystallographic files for **1**–**6** in CIF format: CCDC 1057602–1057606 and 1058046, respectively.

Acknowledgements

This work was financially supported by the National Natural Science Foundation of China (Project 21201091) and the Fundamental Research Funds for the Central Universities (Project lzujbky-2013-59). AMK acknowledges the Foundation for Science and Technology (FCT), Portugal (PTDC/QUI-QUI/121526/2010, PEst-OE/QUI/UI0100/2013).

References

1 J. B. DeCoste and G. W. Peterson, *Chem. Rev*., 2014, **114**, 5695.

2 J. Liu, L. Chen, H. Cui, J. Zhang, L. Zhang and C. Y. Su, *Chem. Soc. Rev*., 2014, **43**, 6011.

3 M. Kurmoo, *Chem. Soc. Rev*., 2009, **38**, 1353.

4 M. W. Zhang, M. Bosch and H. C. Zhou, *CrystEngComm*, 2015, **17**, 996.

5 H.C. Zhou, J.R. Long and O.M. Yaghi, *Chem. Rev*., 2012, **112**, 673.

6 A. G. Wong-Foy, A. J. Matzger and O. M. Yaghi, *J. Am. Chem. Soc*., 2006, **128**, 3494.

7 S. Shimomura, M. Higuchi, R. Matsuda, K. Yoneda, Y. Hijikata, Y. Kubota, Y. Mita, J. Kim, M. Takata and S. Kitagawa, *Nat. Chem*., 2010, **2**, 633.

8 G. R. Desiraju, *J. Am. Chem. Soc*., 2013, **135**, 9952.

9 O. F. Sun, J. Iwasa, D. Ogawa, Y. Ishido, S. Sato, T. Ozeki, Y. Sei, K. Yamaguchi and M. Fujita, *Science*, 2010, **328**, 1144.

10 Z. Z. Lu, R. Zhang, Y. Z. Li, Z. J. Guo and H. G. Zheng, *J. Am. Chem. Soc*., 2010, **133**, 4172.

11 L. N. Zhang, C. Zhang, B. Zhang, C. X. Du and H. W. Hou, *CrystEngComm*, 2015, **17**, 2837.

12 M. Du, C. P. Li, C. S. Liu and S. M. Fang, *Coord. Chem. Rev*., 2013, **257**, 1282.

13 X. M. Chen and M. L. Tong, *Acc. Chem. Res*., 2007, **40**, 162.

14 R. Singh and P. K. Bharatdwaj, *Cryst. Growth Des*., 2013, **13**, 3722.

15 A. Stepenson and M. D. Ward, *Chem. Commun*., 2012, **48**, 3605.

16 J. Z. Gu, Z. Q. Gao and Y. Tang, *Cryst. Growth Des.*, 2012,**12**, 3312.

17 J. Z. Gu, A. M. Kirillov, J. Wu, D. Y. Lv, Y. Tang and J. C. Wu, *CrystEngComm.*, 2013, **15**, 10287.

18 Z. J. Wang, L. Qin, X. Zhang, J. X. Chen and H. G. Zheng, *Cryst. Growth Des.*, 2015, **15**, 1303.

19 S. Tripathi and G. Anantharaman, *CrystEngComm*, 2015, **17**, 2754.

20 J. Z. Gu, D. Y. Lv, Z. Q. Gao, J. Z. Liu, W. Dou and Y. Tang, *J. Solid State Chem.*, 2011,**184**, 675−683.

21 H. Y. Liu, H. Wu, J. Yang, Y. Y. Liu, B. Liu and J. F. Ma, *Cryst. Growth Des.*, 2011, **11**, 2920.

22 X. T. Zhang, L. M. Fan, W. L. Fan, B. Li and X. Zhao, *CrystEngComm*, 2015, **17**, 6681.

23 H. Y. Li, L. H. Cao, Y. L. Wei, H. Xu and S. Q. Zang, *CrystEngComm*, 2015, **17**, 6297.

24 M. L. Han, L. Bai, P. Tang, X. Q. Wu, Y. P. Wu, J. Zhao, D. S. Li and Y. Y. Wang, *Dalton Trans*., 2015, **44**, 14673.

25 J. Zhao, G. H. Zhu, L. Q. Xie, Y. S. Wu, H. L. Wu, A. J. Zhou, Z. Y. Wu, J. Wang, Y. C. Chen and M. L. Tong, *Dalton Trans*., 2015, **44**, 14424.

26 Z. Q. Gao, H. J. Li and J. Z. Gu, *Chinese Inorg. Chem.*, 2014, **30**, 2803.

27 L. V. Tsymbal, I. L. Andriichuk, Ya. D. Lampeka and V. B. Arion, *J. Struct. Chem.*, 2014, **55**, 1466.

28 W. Q. Zhang, J. C. Yu, Y. J. Cui, X. T. Rao, Y. Zhang and G. D. Qian, *J. Alloys Comp.*, 2013, **551**, 616.

29 G. Labbé, A. P. Krismanich, S. de Groot, T. Rasmusson, M. H. Shang, M. D. R. Brown, G. I. Dmitrienko and J. G. Guillemette, *J. Inorg. Biochem.*, 2012, **112**, 49.

30 (*a*) G. M. Sheldrick, *Acta Crystallogr.*, 1990, **A 46**, 467; (*b*) G. M. Sheldrick, SHELXS-97*, A Program for X-ray Crystal Structure Solution*, *and SHELXL-97, A Program for X-ray Structure Refinement*, Göttingen University, Germany, 1997.

31 (*a*) V. A. Blatov, *IUCr CompComm Newsletter*, 2006, **7**, 4; (*b*) V. A. Blatov, A. P. Shevchenko and D. M. Proserpio, *Cryst. Growth Des*., 2014, **14**, 3576.

32 The Reticular Chemistry Structure Resource (RCSR) Database; M. O'Keeffe, M. A. Peskov, S. J. Ramsden and O. M. Yaghi, *Acc. Chem. Res*., 2008, **30**, 1782.

33 See the Cambridge Structural Database (CSD, version 5.36, 2015): F. H. Allen, *Acta Crystallogr*., 2002, **B58**, 380.

34 F. Y. Yi and Z. M. Sun, *Cryst. Growth Des*., 2012, **12**, 5693.

35 (*a*) M. O'Keeffe and O. M. Yaghi, *Chem. Rev*., 2012, **112**, 675; (*b*) M. Li, D. Li, M. O'Keeffe and O. M. Yaghi, Chem. Rev., 2014, **114**, 1343.

36 P. Van der Sluis and A. L. Spek, *Acta Crystallogr., Sect. A: Found. Crystallogr*., 1990, **46**, 194.

37 D. Sun, L. L. Han, S. Yuan, Y. K. Deng, M. Z. Xu and D. F. Sun, *Cryst. Growth Des.*, 2013, **13**, 377.

38 Y. Zhang, B. B. Guo, L. Li, S. F. Liu and G. Li, *Cryst. Growth Des.*, 2013, **13**, 367.

39 W. Hiller, J. Strähel, A. Datz, M. Hanack, W. E. Hatfield, L. W. Ter Haar and P.

Gütlich, *J. Am. Chem. Soc.*, 2009, **131**, 10140.

40 (a) K. F. Hsu and S. L. Wang, *Inorg. Chem*., 2000, **39**, 1773; (b). O. Kahn, *Molecular Magnetism*; VCH Publishers Inc.: New York, 1993; p 211.

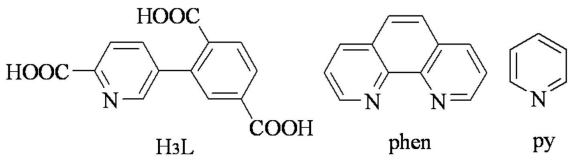

Scheme 1 Structural formulae of ligands used in this work.

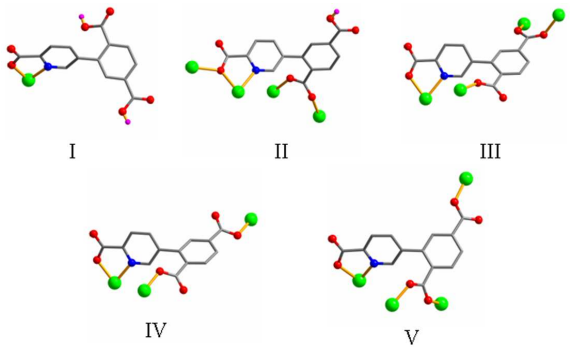

Scheme 2 Various coordination modes of H_2L^- / HL^{2-} / L^{3-} in compounds **1**–**6**.

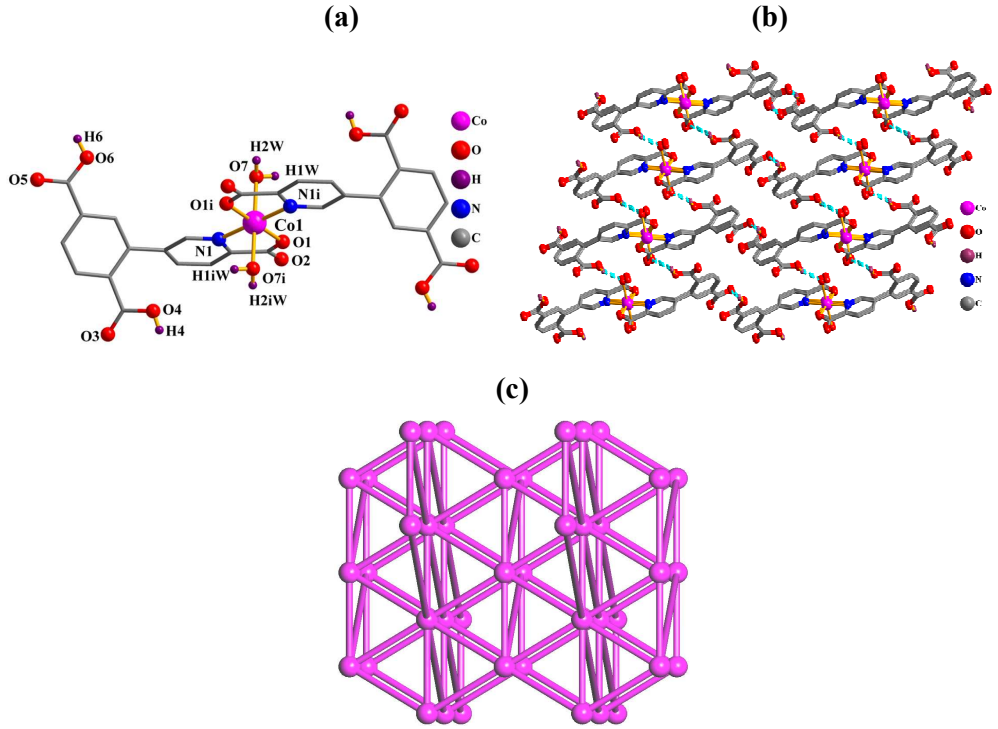

Fig. **1** Structural fragments of **1**. (a) Coordination environment of the Co(II) atom. Symmetry code: i = $-x + 2$, $-y + 1$, $-z + 1$. (b) Perspective of the 3D H-bonded framework along the *ac* plane (blue dashed lines represent the H-bonds). (c) Topological representation of the underlying 3D H-bonded framework showing a uninodal 8-connected net with the **8T9** topology; view along the *a* axis; color codes: centroids of 8-connected $[Co(H_2L)_2(H_2O)_2]$ molecular nodes (magenta).

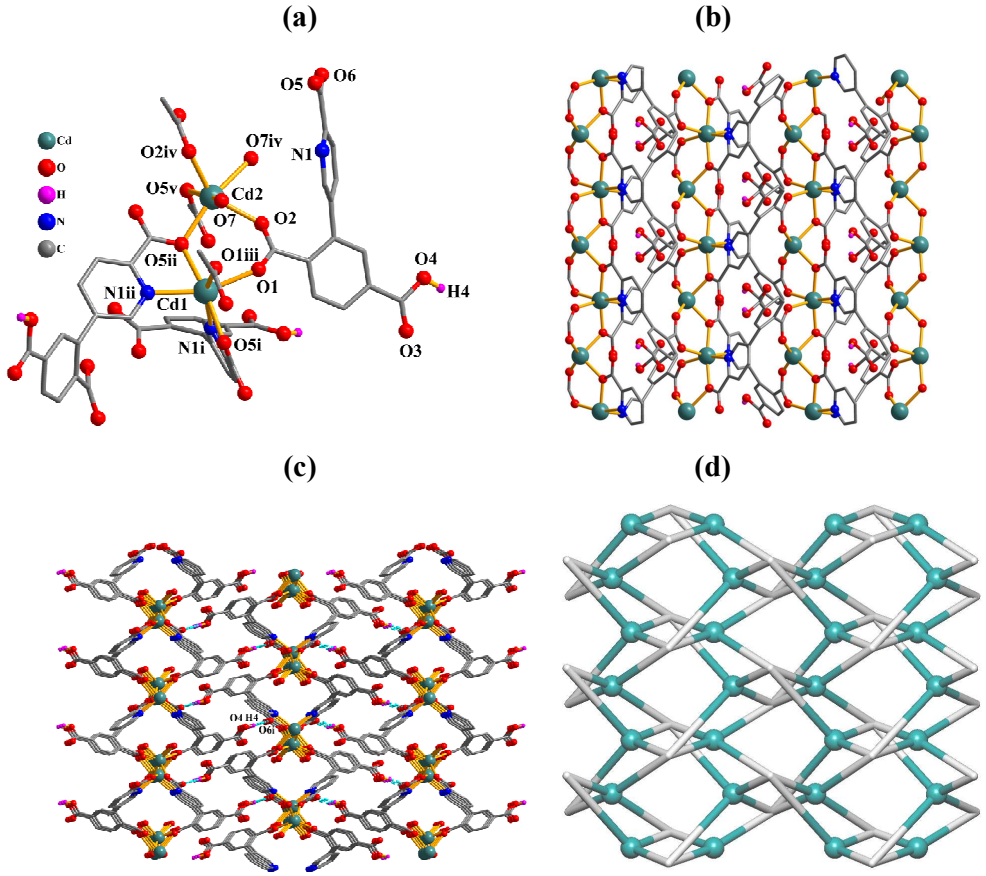

Fig. **2** Structural fragments of **2**. (a) Coordination environment of the Cd(II) atoms. Symmetry codes: i = *x* + 1/2, *y*, –*z* + 2; ii = *x* + 1/2, –*y* + 1/2, *z* + 1/2; iii = *x*, –*y* + 1/2, –*z* + 5/2; iv = *x*, –*y* + 1/2, –*z* + 3/2; v = *x* + 1/2, *y*, –*z* + 1. (b) Perspective of the 2D metal-organic sheet along the *ac* plane. (c) Perspective of the 3D supramolecular framework along the *ab* plane (blue dashed lines represent the H-bonds). Symmetry code: i = –*x* + 3/2, –*y* + 1, *z* + 1). (d) Topological representation of the underlying 2D metal-organic network showing a binodal 4,4-connected layer with the unique topology defined by the point symbol of $(4^3.6^2.8)$; view along the *b* axis; color codes: 4-connected Cd1 and Cd2 nodes (turquoise), centroids of 4-connected μ_4-HL nodes (gray).

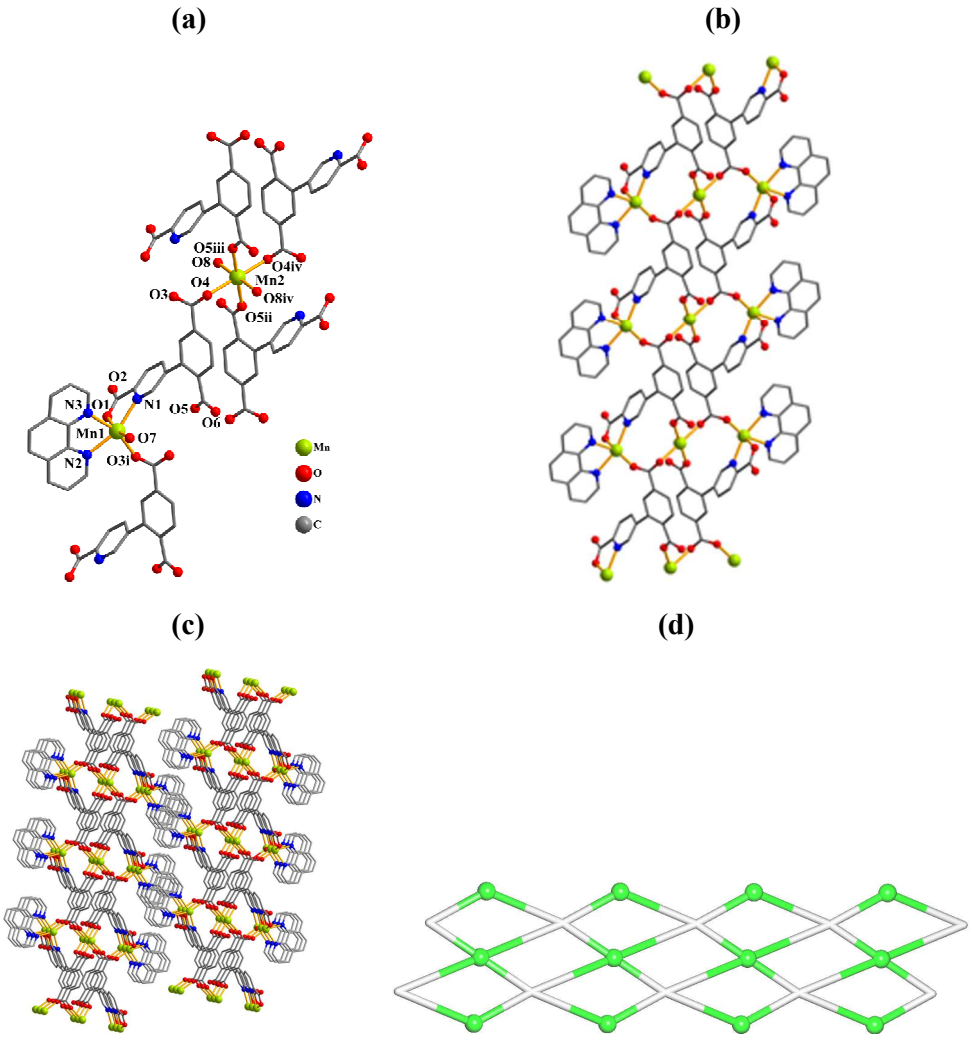

Fig. 3 Structural fragments of **4**. (a) Coordination environment of the Mn(II) atoms. Symmetry codes: i = *x*, *y* – 1, *z*; ii = –*x* + 1, –*y* + 2, –*z* + 1; iii = *x*, *y* + 1, *z*; iv = –*x* + 1, –*y* + 3, –*z* + 1. (b) Perspective of a 1D metal-organic chain along the *bc* plane. (c) Perspective of a 3D supramolecular framework along the *bc* plane. (d) Topological representation of the underlying 1D metal-organic network showing a binodal 4,4-connected chain with the unique topology defined by the point symbol of $(3^2.4.5^2.6)_2(3^2.4^2.5^2)$; view along the *a* axis; color codes: 2-connected Mn1 linkers and 4-connected Mn2 nodes (green), centroids of 4-connected μ_4-L nodes (gray).

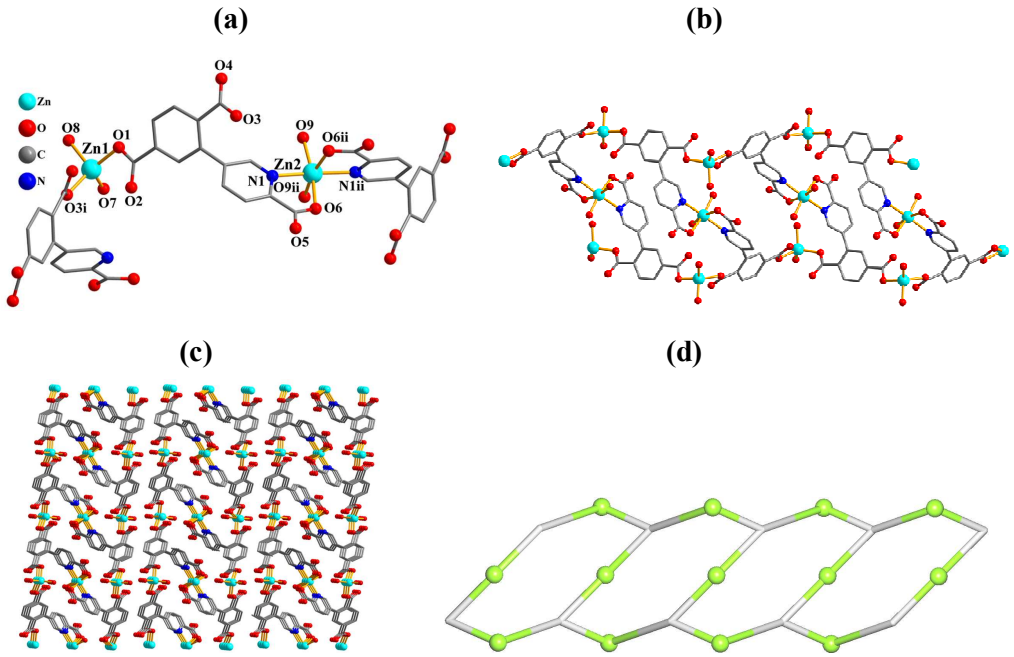

Fig. 4 Structural fragments of **5**. (a) Coordination environment of the Zn(II) atoms. Symmetry codes: i = x, $-y + 1$, $z - 1/2$; ii = $-x + 1$, y, $-z + 3/2$. (b) Perspective of a 1D ladder-like metal-organic chain along the *ac* plane. (c) Perspective of a 3D supramolecular framework along the *ac* plane. (d) Topological representation of the underlying 1D metal-organic network showing a uninodal ladder-like 3-connected chain with the SP 1-periodic net (4,4)(0,2) topology; view along the *b* axis; color codes: 2-connected Zn1 and Zn2 linkers (pale green), centroids of 3-connected μ_3-L nodes (gray).

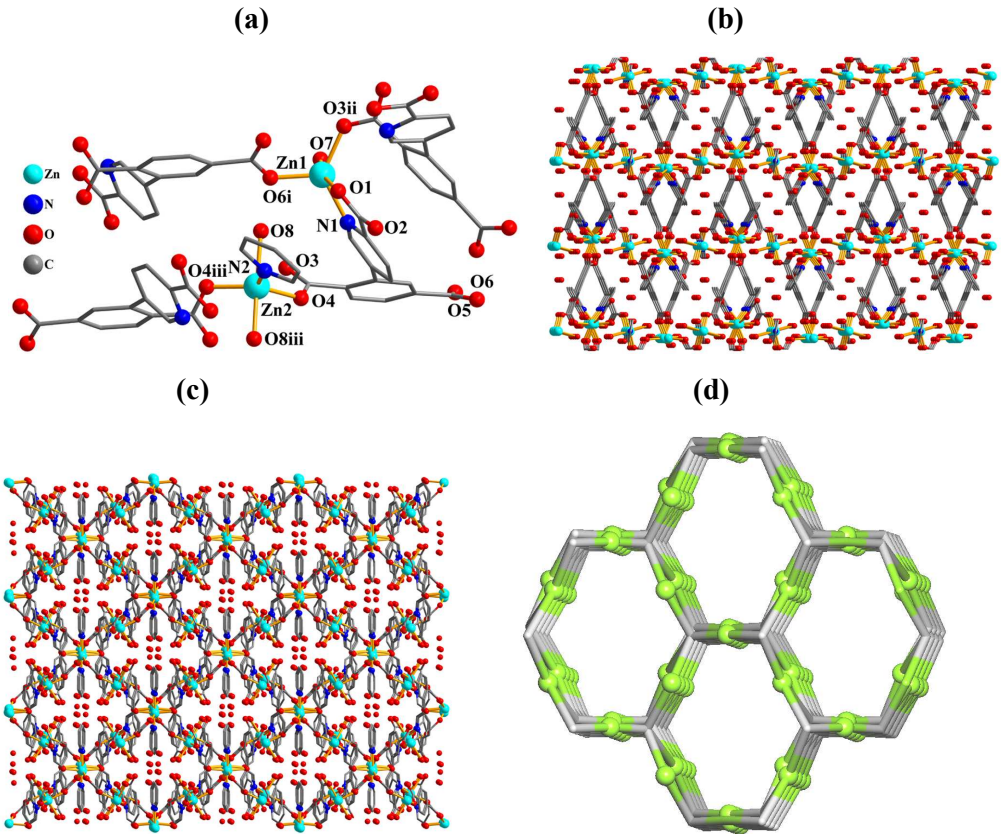

Fig. **5** Structural fragments of **6**. (a) Coordination environment of the Zn(II) atoms. Symmetry codes: i = x, $-y + 1$, $z + 1/2$; ii = $-x + 1/2$, $y + 1/2$, z; iii = $-x + 1$, y, $-z + 1/2$. (b) Perspective of the 3D porous framework along the *ac* plane. (c) Perspective of the 3D porous framework along the *ab* plane. (d) Topological representation of the underlying 3D metal-organic framework showing a binodal 3,4-connected net with the fsc-3,4-Pbcn-2 topology; view along the *c* axis; color codes: 2-connected Zn2 linkers and 3-connected Zn1 nodes (pale green), centroids of 4-connected μ_4-L nodes (gray).

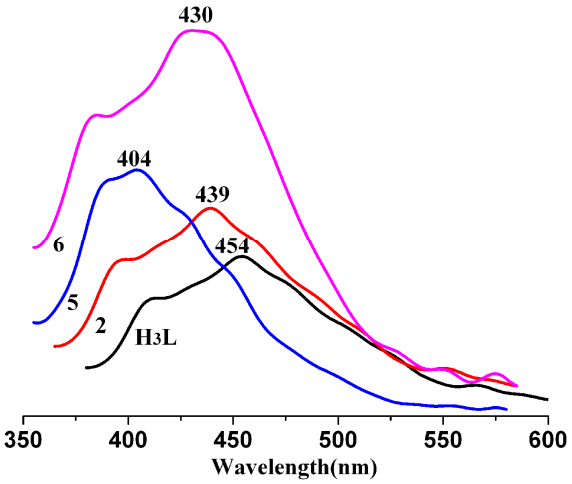

Fig. **6** Solid state emission spectra of H_3L, **2**, **5**, and **6** (λ_{ex} of 365, 352, 345, and 341 nm, respectively).

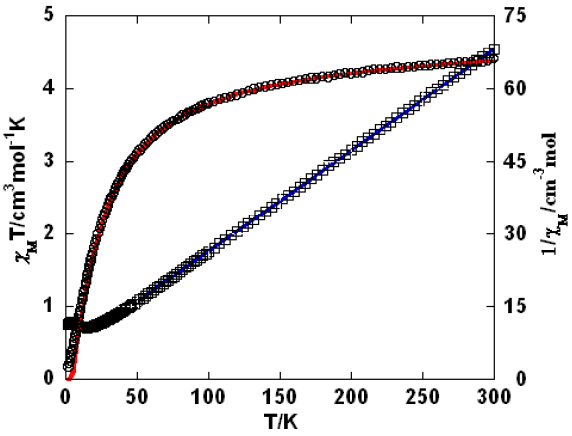

Fig. **7** Temperature dependence of $\chi_M T$ (O) and $1/\chi_M$(□) vs. *T* for compound **3**. The red line represents the best fit to the equations in the text. The blue line shows the Curie-Weiss fitting.

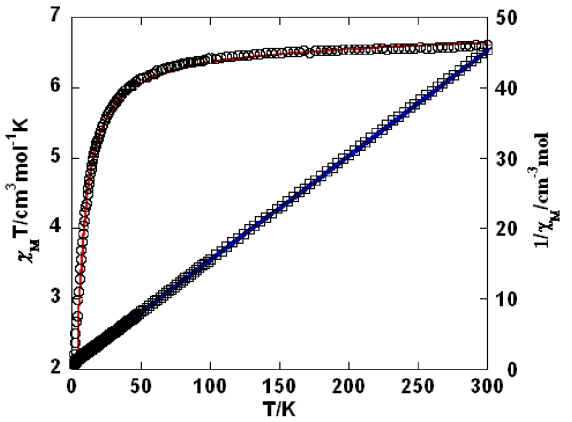

Fig. **8** Temperature dependence of $\chi_M T$ (O) and $1/\chi_M$(□) vs. *T* for compound **4**. The red line represents the best fit to the equations in the text. The blue line shows the Curie-Weiss fitting.

Table 1 The crystallographic data for **1**–**6**.

Compound	**1**	**2**	**3**	**4**	**5**	**6**
Chemical formula	$C_{28}H_{20}CoN_2O_{14}$	$C_{14}H_9CdNO_7$	$C_{14}H_9MnNO_7$	$C_{26}H_{20}Mn_{1.5}N_3O_9$	$C_{28}H_{24}Zn_3N_2O_{18}$	$C_{33}H_{33}Zn_3N_3O_{20}$
Formula weight	667.39	415.62	358.16	600.86	872.60	987.73
Crystal system	Monoclinic	Orthorhombic	Orthorhombic	Triclinic	Monoclinic	Orthorhombic
Space group	$P2_1/c$	*P*nna	*P*nna	*P*-1	*C*2/c	*P*bcn
a/Å	16.9118(11)	14.481(4)	14.5661(10)	7.226(8)	29.702(3)	15.5051(7)
b/Å	6.8877(6)	25.238(7)	25.0223(17)	10.388(12)	6.1660(3)	12.2437(5)
c/Å	11.8438(10)	7.5208(19)	7.4491(6)	17.46(2)	16.6016(8)	18.0992(5)
α/°	90	90	90	104.832(14)	90	90
β/°	105.872(9)	90	90	93.230(12)	94.853(6)	90
γ/°	90	90	90	104.588(13)	90	90
V/Å^3	1327.00(18)	2748.5(12)	2715.0(3)	1216(2)	3029.5(3)	3436.0(2)
T/K	293(2)	296(2)	293(2)	296(2)	291(2)	293(2)
Z	2	8	8	2	4	4
D_c/g cm^{-3}	1.670	2.009	1.752	1.641	1.913	1.909
μ/mm^{-1}	0.729	1.628	1.012	0.854	2.448	2.176
F(000)	682	1632	1448	613	1760	2008
Refl. measured	4550	18100	6744	8606	3310	9140
Unique refl. (R_{int})	2343 (0.0495)	2427 (0.0210)	2401 (0.0389)	4153 (0.0372)	3310 (0.0806)	3029(0.0486)
GOF on F^2	1.064	1.044	1.026	1.048	0.95	1.058
R_1 [$I > 2\sigma(I)$][a]	0.0510	0.0234	0.0412	0.0443	0.0395	0.0463
wR_2 [$I > 2\sigma(I)$][b]	0.0902	0.0633	0.0975	0.1110	0.0784	0.1185

A variety of metal-organic and supramolecular networks constructed from a new flexible multifunctional building block bearing picolinate and terephthalate functionalities: hydrothermal self-assembly, structural features, magnetic and luminescent properties

Yong-Liang Shao,[a] Yan-Hui Cui,[a] Jin-Zhong Gu,*[a] Alexander M. Kirillov,[b] Jiang Wu[a] and Ya-Wen Wang*[a]

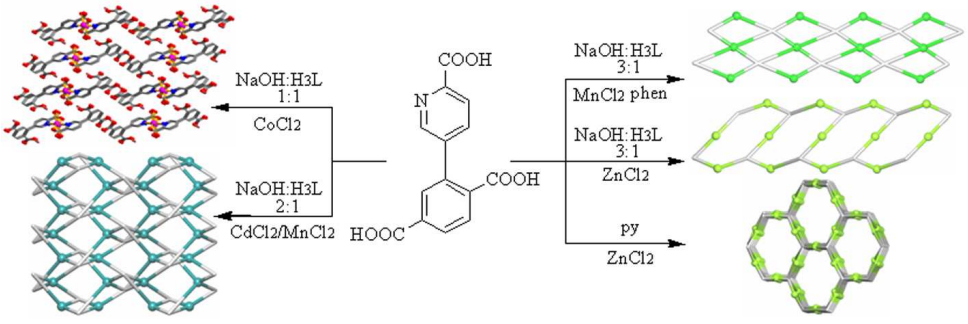

A novel multifunctional flexible organic building block was designed and applied for the hydrothermal self-assembly generation of a new series of polymeric or discrete coordination compounds; their structural and topological features as well as magnetic and luminescent properties were investigated.